Fusion reactions from >150 keV ions in a dense plasma focus plasmoid

Eric J. Lerner, S. Krupakar Murali, Derek Shannon, Aaron M. Blake, and Fred Van Roessel
Lawrenceville Plasma Physics, 128 Lincoln Blvd., Middlesex, New Jersey 08846-1022, USA

Using a dense plasma focus device with a 50 kJ capacitor charge, we have observed fusion reactions from deuterium ions with record energies of >150 keV, which are confined for durations of 7–30 ns in the cores of plasmoids with typical radii of 300–500 μm and densities $\sim 3 \times 10^{19}$ cm^{-3}. We have for the first time simultaneously imaged the plasmoid at high (30 μm) resolution and measured trapped ion energy and neutron anisotropy. The isotropy of the neutron emission as well as other observations confirms that the observed neutrons per pulse of up to 1.5×10^{11} are produced mainly by confined ions, not an unconfined beam. The conditions achieved are of interest for aneutronic fusion, such as with pB11 fuel. © 2012 American Institute of Physics.
[http://dx.doi.org/10.1063/1.3694746]

I. INTRODUCTION

The dense plasma focus (DPF) device has long been known to be an efficient source of neutrons from fusion reactions and of MeV-energy ion and electron beams.[1,2] It also produces dense concentrations of hot plasma, or plasmoids.[3–5] However, there have been a number of key unresolved questions that are debated and which have major importance for the possibility of using the DPF as a future source of fusion energy. First, do the neutrons primarily come from high-energy ions that are confined in a dense plasmoid, or from an unconfined ion beam's collision with either background gas or a cool plasmoid? Second, are the high-energy ions present only in the beam, or are they also trapped and circulating in the plasmoids? Third, what are the typical dimensions of the plasmoids—centimeters, tens to hundreds of micrometers, or in between?

These questions are closely linked, since only trapped high-energy ions could produce large numbers of neutrons in the plasmoids. In addition, only plasmoids with relatively small volumes and masses could be heated to high average ion energies with the total energy available in the device. Researchers such as Brzosko, Bostick, and Nardi[6,7] have reported small plasmoids, radius <1 mm, with trapped ions with typical energy >50 keV and most of the neutrons coming from the confined ions, while others such as Kubes[8] have reported large plasmoids, radius >1 cm, with ions not confined or only partially confined (for a few orbits) and most neutrons from interactions with a beam.

These questions are of high practical interest, since if high-energy ions are trapped in the plasmoids, it is possible that with suitable conditions and fill gases, the energy released by fusion reactions could also be trapped, leading to ignition of the fusion fuel and high fusion yields. This would not be possible if the fusion reactions are mainly coming from a single pass of an ion beam.

Our experiments using a DPF with small-radius electrodes have given clear answers to these questions. We have observed a record 900 keV full-width half-maximum (FWHM) spread in neutron energies from deuterium reactions, which implies average ion energies as high as 160 keV for Maxwellian plasma,

and higher if the high-energy ions are not yet thermalized. integrated charge-coupled device (ICCD) images, low anisotropy in neutron production, energy considerations, and the strong correlation of ion energy with fusion power all combine to demonstrate that >70% of the 10^{11} neutrons in the hottest shots are produced by ions confined in small plasmoids with core radii of 300–500 μm. We believe this result does not contradict other results obtained previously, such as by Kubes,[8] but is mainly the result of the relatively small radii of our electrodes, which lead to higher densities in the plasmoid and more effective heating of the ions.

A. The DPF—background of present work

The DPF is a compact and simple device first developed in the 1960s by N. V. Filippov in the USSR and by J. W. Mather in the USA and has been studied by dozens of groups over the last 45 years, resulting in a large and rich literature. It consists of two concentric cylindrical electrodes enclosed in a vacuum chamber. The chamber is evacuated to low pressure and then backfilled to several Torr with the fuel gas. A pulse of electricity with a rise time of 0.2–10 μs from a capacitor bank is discharged across the electrodes during operation.[4] In operation, the capacitors discharge in a several-microsecond pulse, the gas is ionized and a current sheath consisting of pinched current filaments forms and runs down the electrodes. When the sheath reaches the end of the inner electrode (the anode), the filaments pinch together in the center, forming dense, magnetically confined hot spots or plasmoids.[9,10] The plasmoids emit x-rays with energies from several keV to over 100 keV. X-ray pinhole images have demonstrated that the plasmoids can be tiny, with radii of hundreds of micrometers or less.[5,11–13] The plasmoids can have densities in the range of 10^{20}–10^{21} cm^{-3}. These densities were measured by a number of independent methods, including heavy ion and secondary product fusion,[14,15] CO_2 laser scattering,[16] and x-ray line intensities.[17] These plasmoids emit intense beams of accelerated ions and electrons.[18–20] Neutrons from fusion reactions are emitted from the device in large quantities (up to 10^{13}) per shot.

The role of the plasmoids in producing the fusion neutrons and the physical processes involved in their formation and maintenance have been hotly debated among DPF researchers for decades. The model that best fits all the existing data makes the role of the plasmoids central to neutron production. This model, initially developed by Bostick and Nardi,[4] and confirmed by observations of several groups over three decades, was elaborated into a more quantitative theory by one of the present authors.[21–26] In this model, the electron beam transfers part of its energy to the plasmoid electrons, which generate x-rays through collisions with nuclei. Through plasma instability (probably ion-acoustic), the electrons then transfer part of their energy to the ions, with a typical delay (in our experiments) of ~20 ns. Ion collisions then occur, generating fusion reactions and neutrons.[26] The fusion reactions end when the ion and electron beams have exhausted the magnetic energy that confines the plasmoid, and partially or wholly evacuated the particles in the plasmoid.

The DPF routinely produces hard x-rays and γ-rays indicating the presence of Bremsstrahlung radiation from high-energy electrons colliding with nuclei.[23] Together with independent evidence, this indicated that the hot spots contained ions and electrons at very high energies in the range of interest for advanced fuel fusion.[10,16,17,23–26]

The Bostick-Nardi model[6] describes the DPF as operating by exploiting a series of natural instabilities in the plasma, with each instability further concentrating the plasma and the magnetic fields produced by the currents running through the plasma. In the past few decades, substantial advances have occurred in understanding the basic physics of such instabilities through experiments and observations of space plasma.

In the first instability, the current sheath moving through the plasma between electrodes breaks up into an array of filaments, increasing the density of the plasma and magnetic field strength by a factor of 10–20. The filamentary current sheath, driven by the interaction of its own currents and magnetic field, travels down to the end of the inner hollow electrode, where the filaments converge into a single central pinch region, further concentrating both plasma and magnetic fields. A third instability then kinks the single central filament like an over-twisted phone cord, forming a plasmoid, an extremely dense, magnetically self-confined ball of plasma only tens or hundreds of micrometers across. By this time, the density and magnetic fields of the plasma in this small region are much larger than those present at the start of the process, and a substantial fraction of the energy fed into the device is contained in the plasmoid. A fourth instability causes the magnetic fields at the center of the plasmoid to decrease, and these changing magnetic fields induce an electric field, which generates a beam of electrons in one direction and a beam of ions in the other. The electron beam heats the plasmoid electrons which in turn heat the ions, thus igniting fusion reactions. The energy is released in the ion and electron beams and in a burst of x-ray energy from the heated electrons in the plasmoid.

In addition to its very small size, simplicity, and ability to utilize the inherent plasma instabilities (rather than suppressing them), the DPF also has the advantage that it produces a plasmoid which is extremely dense. Such a dense plasmoid requires that the ions be confined for only a few thousand orbits, in contrast to the millions of orbits required in tokamaks or most other fusion devices. Thus the high stability of such devices is not required in the DPF, but rather only meta-stability.

II. EXPERIMENTAL APPARATUS

The experiments were performed with the "Focus Fusion-1" (FF-1) dense plasma focus at Lawrenceville Plasma Physics' laboratory in Middlesex, NJ.[26] This device is energized by a 113 μF, 12-capacitor bank. The cathode has a radius of 5 cm, and the anode has a radius of 2.8 cm, while in the present configuration both have a length of 14 cm, with a 2.8 cm-long ceramic insulator between them. The shots analyzed here were performed with charging voltages varying from 30 to 36 kV and peak current from 0.7 to 1.1 MA. For such relatively high currents, our electrodes are small, a choice based on theoretical indications that such small electrodes and the associated higher magnetic fields will allow denser and hotter plasmoids.[26] By comparison, mega-amp DPFs in Las Vegas[27] and Warsaw[8] have electrodes close to two and four times our radii, respectively. The fill gas was deuterium and the fill pressure was varied from shot to shot over a range of 10–24 Torr.

The current in FF-1 is measured by digitally integrating a Rogowski coil signal, while the number of neutrons generated are measured by three types of independent sets of instruments: a calibrated silver activation counter located 81 cm from the axis of the device; calibrated bubble detectors located at 90°, 12.5°, and 4° from the axis and on the axis in the direction away from the anode; and by integrating the signals from two time-of-flight (TOF) scintillator-photomultiplier tubes (PMTs) located at 11 m (near time-of-flight, NTF) and 17 m (far time-of-flight, FTF), at 90° from the axis. The rise time of the scintillator (25-mm-thick BC-404) is 2 ns and this is also the rise time of the PMTs. Out of 242 shots fired in the test period of September 1, 2010 to March 1, 2011, 44 shots had high signal-to-noise ratios in both the NTF and FTF detectors, and so they were selected for further analysis here.

In addition, in October 2011, we added a third inner time-of-flight (ITF) detector at an angle of 4° from the axis in the direction that the ion beam travels (downwards from the anode) at a distance of 1.2 m. This detector was shielded on all sides by 5 cm of lead to reduce the x-ray signal. We analyzed an additional 23 shots with similar conditions to the first set: charge voltage 33–40 kV, fill pressure 16–27 Torr, and peak current 0.8–1.0 MA. For these shots, we also had a vertical PMT (VPMT) located on axis above the anode, 32 cm from the tip of the anode.

III. DATA ANALYSIS

A. Time-of-flight data

Data from the TOF PMTs is measured at a 1 sample-per-ns rate by digital oscilloscopes. Figure 1 shows typical (inverted) NTF and FTF signals, showing the x-ray and later neutron pulse arrivals. To minimize shot and electromagnetic (EM) noise, the resulting data files are then averaged over a
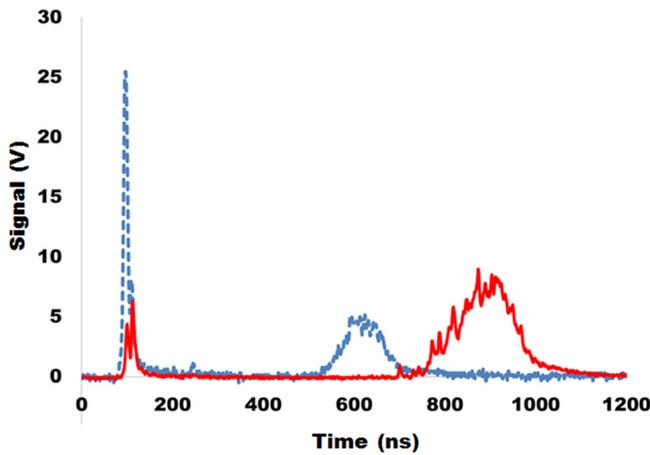
FIG. 1. Inverted data output for shot 11012403 from the Near Time of Flight PMT (dashed) and the Far Time of Flight PMT (solid) showing early x-ray peak and later neutron peak. The larger diameter FTF scintillator is more sensitive to neutrons. The timing of the data is shifted to compensate for photon time of flight and cable delays.

20 ns window for the NTF and FTF signals and over a 5 ns window for the 1.2 m ITF signals.

For the first set of shots, observed with two TOF detectors, we have determined for each shot an average ion energy using the formula,

$$E_i = 2E(W^2 - \tau^2)/t^2,$$

where E_i is the mean ion energy, E is the neutron energy derived from the fusion reaction, t is the time required for a neutron of energy E to travel to the detector, W is the FWHM of the pulse at the detector, and τ is the duration of the neutron pulse at the origin of the pulse. This formula is an accurate fit (within 5%) to numerical values calculated by Bogdanov and Volosov[28] over a range in E_i from 2 to 100 keV assuming a Maxwellian plasma. For a non-Maxwellian distribution, the average energy is higher for the same W, so for the extreme case of a mono-energetic distribution, the same W results from ions at 220 keV, whereas a Maxwellian distribution gives 160 keV. By using the data from both the NTF and FTF, we can solve for both τ and E_i.

We have chosen to report the E_i for an assumed Maxwellian distribution only because these are the lowest and, therefore, most conservative values, not because we believe that the plasmoids are, in most cases, near-Maxwellian. Using these methods, we observed a broad range of E_i (see Table I) with mean $E_i = 72$ keV. Nine shots, 20% of the

TABLE I. Distribution of average ion energies.

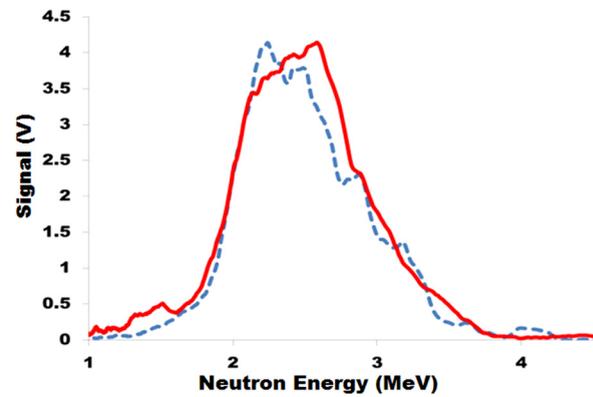| E_i (keV)	FWHM (keV)	Number of shots
0–20	0–320	6
20–40	320–450	7
40–60	450–560	4
60–80	560–650	9
80–100	650–720	9
100–150	720–880	5
>150	>880	4

FIG. 2. Shot 11012403. PMT output for the NTF at 11 m (dashed blue) and FTF at 17 m (solid red) from the device axis plotted against neutron energy, determined from time-of-flight. The signals are recorded every nanoseconds and averaged over 20 ns. The amplitude of the NTF signal is magnified to match the peak height of the FTF signal. The FWHM of 960 ± 40 keV is a record for any DPF. Note the close agreement of the two signals.

total, have $E_i > 100$ keV, and the hottest four shots have $E_i \sim 160$ keV. For ease of comparison with other results, we also give the range of the FWHM of the neutron energy spectra. Fig. 2 shows the TOF signals for one of the 4 hottest shots, shot 11012403, showing a FWHM of >900 keV, a record for a DPF.

(The largest FWHM previously reported, as early as 1978,[29] was 700 keV, or $E_i = 100$ keV.) For the same 44 shots, total neutrons averaged 4×10^{10} with a maximum of 1.1×10^{11} in one shot. While there is a large scatter in the results when plotted against peak current, pressure, or charging voltage, the nine shots with $E_i > 100$ keV occurred within a relatively narrow range of conditions, with charging voltage 32–35 kV, peak current 0.9–1.1 MA and for 8 of the 9 shots, fill pressure of 15–18 Torr, with 5 of the 9 shots occurring at 18 Torr. In addition, the upper envelope of the E_i vs. I distribution (the shots with the largest E_i for a given I) shows a clear increase of E_i with I (see Fig. 3).

When the total number of neutrons generated Y, the duration of the neutron pulse τ, and the neutron rate $P = Y/\tau$ are plotted against E_i, significant correlations are seen (see Fig. 4). For P, there is no correlation with E_i for $E_i < 40$ keV and P is in a relatively narrow range of $2.5–7 \times 10^8$/ns. But for $E_i > 40$ keV and most clearly for $E_i > 70$ keV, there is a
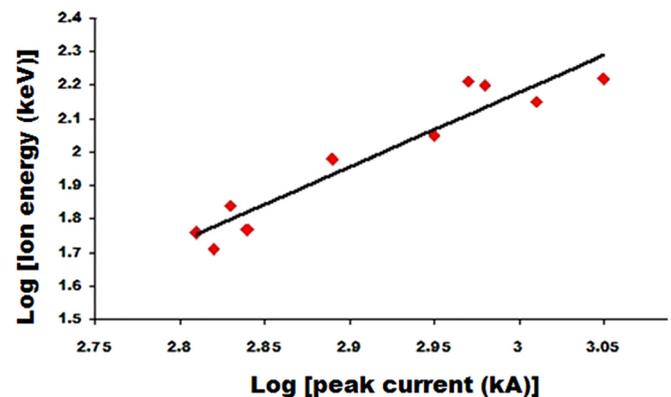

FIG. 3. Ion energy scales as I2 (upper envelope). Line is a linear fit to points with slope of $I^{2.2}$.
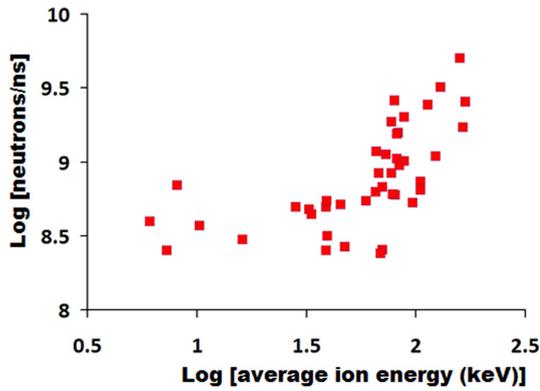
FIG. 4. Correlation between fusion power and average ion energy. Note correlation above around 40 keV and no correlation below that energy. Error bars omitted for clarity.

significant correlation. For the 32 shots with $E_i > 40$ keV, $P = kE_i^{1.4 \pm 0.3}$, with correlation r = 0.65, significant at the 1% level. In the energy range from 40 to 170 keV, the reaction rate for $D + D \rightarrow n + {}^3He$ rises with $E_i^{1.17}$, so the results are consistent with the product $n' n \cdot V$ being independent of E_i, where n' is the number density of the hot ions, n the density of all ions in the region of neutron production, and V the volume of the region. Similar patterns are seen for Y and τ, with no correlation and a narrow range for $E_i < 40$ keV and a significant correlation for $E_i > 40$ keV (see Table II).

To confirm and refine the results that we obtained by using two TOF detectors, we carried out additional experiments with three detectors, using an additional TOF detector at 1.2 m, close to the axis (called the ITF detector). In these cases, we were able to determine τ more accurately, since at 1.2 m the neutrons have not had time to spread out as much as at 11 m. Here we calculated E_i using the ITF and FTF data.

When E_i is calculated in this way, the earlier results are broadly confirmed, but the distribution is shifted to still higher E_i. When these 23 shots are measured using NTF and FTF data, the mean E_i is 72 keV, but when calculated with ITF and FTF data, the mean E_i is 103 keV. With the 12 shots with $E_i > 100$ keV, agreement between the two methods used to measure individual shots is closer, with 6 of these 12 shots having both measures in agreement within 20%. The "hottest" shot in this series had E_i of 170 keV, indistinguishable from the hottest 4 shots of the previous set.

The correlation of P with E_i is again observed with this second data set, using ITF measurements for τ. The relation here for the 22 shots with $E_i > 40$ keV is $P = kE_i^{1.8 \pm 0.3}$ is somewhat steeper than (but in adequate agreement with) that derived from the earlier data, and the correlation r is similar at 0.62.

TABLE II. Correlations of variables on E_i for $E_i > 40$ keV.

Correlation on Log E_i	Slope	r
Log P	1.43 + 0.30	0.65
Log Y	0.83 + 0.27	0.51
Log τ	−0.56 + 0.22	0.42

There is thus convincing evidence that neutrons in FF-1 originate in regions that, in some shots, have ions with mean energy $E_i > 150$ keV.

B. Neutron energy isotropy

Given these high ion energies, the key question is whether they are produced by an unconfined ion beam, with the energy spread perpendicular to the device axis generated by the divergence of the beam, or if instead they are produced by trapped ions that are circulating within a dense plasmoid. A significant experimental test that differentiates these two cases is to compare the mean neutron energy in the axial direction with that in the perpendicular direction (horizontal in the case of FF-1). For ions trapped in a plasmoid, we expect the neutron energies to be equal and thus the neutron anisotropy to be zero. However, if the neutrons are primarily produced by the axial ion beam, the average neutron energy in the direction of that beam will significantly exceed the mean energy perpendicular to the beam, so energy anisotropy will differ from zero.

We have used the axial signals from the ITF detector to measure the mean axial neutron energy and from the NTF and FTF to measure the mean perpendicular neutron energy (E_p). The mean neutron velocity and thus E_p can be measured directly from the difference in the peak arrival time at the NTF and FTF. The velocity derived and the timing information then yield the time of origin of the neutron pulse. That time, together with the measured time of arrival of the neutron pulse at the ITF detector, then yield the axial velocity and thus axial neutron energy (E_a).

For the 23 shots from October 2011, mean E_p is 2.25 ± 0.03 MeV and mean E_a is 2.65 ± 0.45 MeV. There is no statistically significant anisotropy. The much larger statistical error for E_a is due to the uncertainty in projecting back the time of origin of the neutrons from the NTF and FTF data, but the value measured is completely consistent with a stationary source value E_0, of 2.45 MeV. There is a significant difference between mean E_p and E_0, but it implies a mean bulk velocity of the neutron source of only 0.087 cm/ns. This would give the deuterons only 8 keV of energy, which is small compared to the up to 160 keV energy inferred from the TOF data. So this test is much more consistent with a neutron origin in trapped ions rather than in an unconfined axial beam.

C. Neutron flux anisotropy

A second key test of a beam vs. confined-ion origin for the neutrons is neutron flux anisotropy. Since a beam of deuterons will produce an anisotropic distribution of neutron flux while trapped ions will produce an isotropic flux distribution, measurement of neutron flux is a sensitive discriminator between the beam and trapped ion origins. Indeed such a test can put quantitative limits on the proportion of total neutron yield which is produced by a beam, if the beam energy is known.

We measured the mean ion energy in the beam (E_b) using the signal from a Rogowski coil located 31 cm from the end of the anode.[30] Since the ion beam is tightly

TABLE III. Neutron flux anisotropy ratio relative to 90°.

	Detector location (degrees from axis)		
E_i (keV)	12.5	4	0
<40	1.16 ± 0.21	2.42 ± 0.31	3.67 ± 1.32
40–100	0.82 ± 0.26	2.17 ± 0.38	1.04 ± 0.38
>100	1.10 ± 0.26	2.41 ± 0.24	1.95 ± 0.62

collimated and is not always exactly aligned with the axis, we succeeded in measuring the beam passing through the Rogowski coil in only 12 shots during May 2011. In these shots, the mean E_b was 320 keV, with the shots with highest yield having $E_b \sim 500$ keV. We can use this value as a rough indicator of the beam energy in other shots.

We compared the flux measured by bubble detectors at 12.5, 4, and 0° (a position directly below the bottom of the drift tube and anode), with that measured by bubble detectors located at 90° from the device axis. As shown in the first column of Table III, there is no statistically significant difference in flux between 12.5 and 90° for shots in any E_i group. We can compare the one-sigma upper limit for the anisotropy of the "hottest" shots of 1.36 with the anisotropy we expect if all the neutrons were produced by an unconfined axial beam colliding with a dense plasmoid near the anode's end.

For a beam energy of 500 keV, the expected anisotropy is 2.6, so we can set an approximate upper limit on the proportion of neutrons produced by a beam colliding with a plasmoid at 23%. Of course the data are also consistent with no anisotropy and thus none of the neutrons coming from an unconfined beam, although at least some neutrons must originate in this way.

The data also excludes the case that a major portion of the neutrons are generated by collisions of the ion beam with background plasma in the vacuum chamber or the 100 cm drift tube that extends below the chamber. Since the bubble detectors at 0° and 4° are necessarily located close to the plasma in the drift tube (at a distance of 8 cm in the case of the 4° detector), they are particularly sensitive to ions in the beam interacting with background plasma very near to their location. By comparison, the 90° detectors are located between 40 cm and 416 cm from the device axis. We took these differences into account by calculating the expected neutron flux from a beam of 500 keV interacting with the background plasma. From a beam that goes all the way down the drift tube, we expect a neutron flux of 1.6×10^{-22} n_pN neutrons/sr at 0° where n_p is the background plasma density and N is the number of beam particles, while at 90° we expect only 5.4×10^{-25} n_pN neutrons/sr from this same source or 300 times less flux. Thus given that the average flux ratio between 0° and 90° actually observed is only 2 (third column of Table III), we expect that no more than 0.3% of the neutrons observed at 90° can come from a beam that extends all the way down the drift tube. Indeed, there is evidence from the pattern of damage caused by ion beam erosion on the base of the vacuum chamber that most of the beam power is not close enough to the axis of the device to travel far down the drift tube.

A second possibility is the generation of neutrons from a beam that only traverses the 16 cm from the end of the anode to the bottom of the vacuum chamber, but is not close enough to the axis to go down the drift tube. In this case, we calculate that the neutron flux would be 4.2×10^{-25} n_pN neutrons/sr at the 12° detector at 28 cm from the anode tip and 7.5×10^{-26} n_pN neutrons/sr for the 90° detector. Thus we could expect a flux anisotropy ratio at 12° of 5.57 if all the neutrons were from the 16-cm long beam. This is far above the maximum of 1.36 anisotropy actually measured, so only about 8% of the neutrons could come from a beam-background interaction.

We thus conclude that at most 30% of the neutrons observed could have come from an unconfined beam and that thus at least 70% of the neutrons come from confined high-energy ions.

D. Timing of neutron emission and beams

It is useful to know when the neutrons are emitted relative to the time of beam generation. We record relatively hard x-rays with the NTF, filtered by 6 mm of copper, through a collimator which restricts the view to the plasmoid, excluding the region where the electron beam hits the anode. However, there is frequently more than one x-ray peak, so identification of a given peak with the beam is not easy. For this purpose, the signal from the VPMT, located above the anode, is relevant, as it is shielded by 14 cm of copper and 5 cm of steel, so is sensitive only to >1 Mev γ-rays generated by the electron beam, as well as to neutrons. The first peak from the VPMT therefore identifies the time of the beam emission.

Looking at the 11 shots in October 2011 with the highest charging potential of 40 kV, we found that the first peak from the VPMT corresponded closely in time with the first x-ray peak observed by the NTF with a time delay of 0 ± 8 ns.

We can then compare the time of beam emission with the peak of neutron emission, as observed in the second, much broader peak from the VPMT. For these 11 shots, the delay of the neutron emission is 26 ± 6 ns. Since the VPMT peak is broadened by scattering, it might appear a few nanoseconds late, so we can also use the time of origin of the neutrons projected back from the NTF and FTF peaks, as in Sec. III B of this paper. The results are similar, with a delay of 32 ± 17 ns, with the increased scatter due to the uncertainty in the back-projection of the neutron origin time.

Since the beam peak FWHM is only 8 ns, this data shows that the neutrons originate close to, but distinctly after the beam, again consistent with an origin of the neutrons from trapped ions, not an unconfined beam colliding with a target. However, the data does not exclude the possibility that the neutrons originate from beam ions that are trapped for tens of nanoseconds in the plasmoids. Nor do the data exclude the possibility that a subsequent smaller beam, after the main one, could be involved in the neutron production.

We show in Figure 5 x-ray data from NTF and x-ray and neutron signals from VPMT for a single shot 11101003,
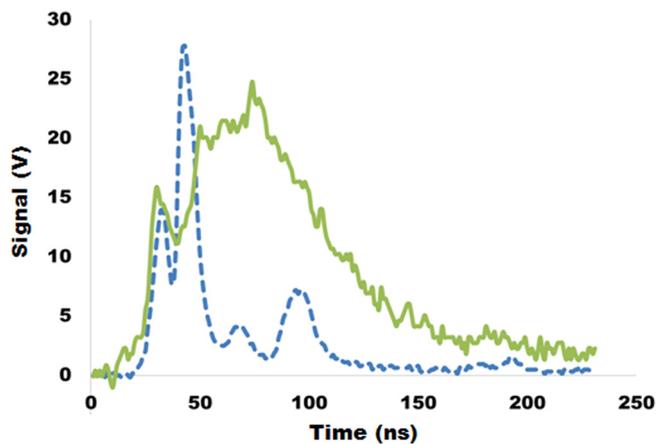
FIG. 5. Signals for shot 11101003 from near time of flight PMT (dashed blue), collimated to view only the region around the plasmoid, and VPMT (solid green), located on axis above the anode and shielded by 14 cm of copper and 5 cm of steel. Signals are corrected for light time of flight and cable delays to refer to origin. Note synchronicity of first peaks, showing electron beam generation. Second broad VPMT peak is for neutrons, broadened by scattering and delayed 13 ns by neutron time-of-flight.

which had the highest neutron yield of the series, 1.5×10^{11} neutrons.

E. Size and density of confined plasma

Given that the hot ions are confined, the next question is what is the size of the region in which they are confined? Images from the ICCD camera allow us to determine the upper limits for the volume of hot plasma in the plasmoid. Because of variability in the exact time of formation of the plasmoids from shot to shot, we observed the plasmoids only in some cases, such as shot 11012403, the same shot when we obtained the record neutron spectral width shown in Figure 2. Figure 6(a) shows the plasmoid formed on axis at a time within 2 ns of the peak x-ray emission and 52 ns prior to the peak of neutron emission. This is the highest-resolution image of a DPF plasmoid yet obtained. This image appears to show the plasmoid core consisting of a coil of plasma filaments. The bright filament is $\sim 60 \mu$m in diameter and is wrapped in a coil that is 400μm in diameter and 1.5 mm long. There is also a 500-μm radius halo of less dense filaments surrounding the inner core. This gives a maximum volume for the hot plasma of $\sim 1.2 \times 10^{-3}$ cm^3. This has to be considered an upper limit for the true volume of hot plasma for two reasons. First, the image was taken well before the peak of neutron production, so the plasmoid was still contracting at this time. Second, the image, taken in visible and UV light, shows the outermost layer of the hot plasma, so the inner, hotter layers have less volume.

Similar images with comparable volumes were obtained in several other shots, including shot 11100604 (Figure 6(b)), which also had a high E_i of 110 keV. Thus, in FF-1, the plasmoids are characterized by dense cores that are on the order of 500μm in radius and 1-2 mm in length.

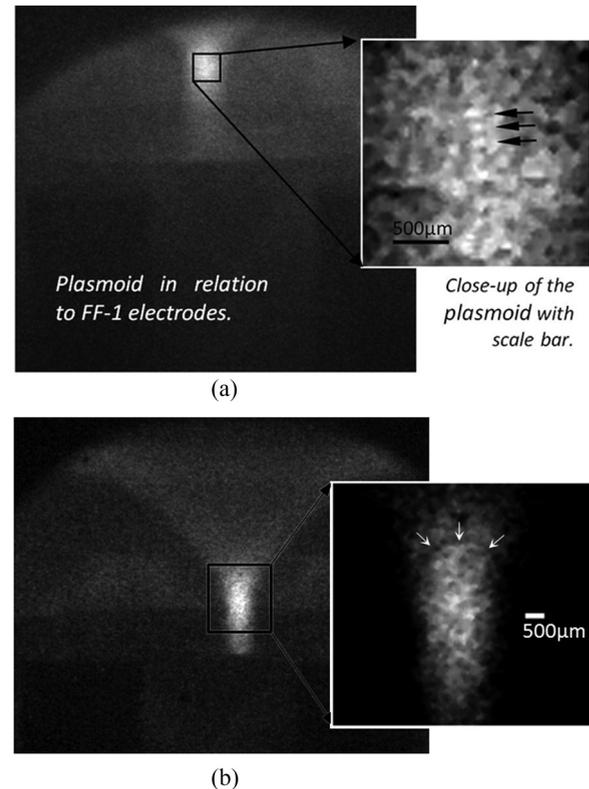With either the Maxwellian assumption, for the known reaction rates for deuterons at a given temperature $T = E_i$, or

FIG. 6. (a) ICCD image of a plasmoid in shot 11012403. Note the filamentary structure, with nearly horizontal 30-μm radius filaments (arrows) wrapped in a 180-μm coil. Exposure 0.2 ns in visible and near-UV. This is the highest-resolution image of a DPF plasmoid yet obtained. (b) 0.2 ns ICCD image of shot 11100604, with a mean ion energy of 110 keV, also shows an approximately 500-μm radius plasmoid. Note shock wave above the plasmoid (arrows), showing sharp resolution of images.

for the assumption of mono-energetic ions confined in a cooler plasma, we find from the observed E_i and Y for the largest shots that the product n^2V is $\sim 4 \times 10^{35}$ cm^{-3}. Given the upper limit of V as about 1.2×10^{-3} cm^3, the lower limit for n is 3×10^{19} cm^{-3}.

We can use the amount of charge emitted in the largest measured ion beams as a minimum measure of nV, the total particle content of the plasmoid, assuming as we do that the beam originates there. Since the largest ion beams we have observed[30] have a total charge of 1.6 mC, nV is around 10^{16}, which makes n $\sim 4 \times 10^{19}$ cm^{-3}, in agreement with our other estimate. We did not perform direct interferometric measurements of the density, but the agreement of the two indirect estimates gives us confidence that they are roughly accurate.

Since ions with 150 keV energy have velocities of 0.37 cm/ns, in 30–40 ns of confinement time, they can be expected to travel ~ 10 cm or at least ~ 30 orbits of the plasmoid. They are fully confined, but a high degree of stability is not required for the observed lifetime of the plasmoids. It seems unlikely, although not impossible, that the ions are in fact fully Maxwellian. For $E_i = 160$ keV and n $= 3 \times 10^{19}$ cm^{-3}, the thermalization time would be about 40 μs, much longer than either the 20 ns between the time of the last x-ray pulse and the peak of the neutron pulse, or the 30–40 ns duration of the neutron pulse.

To summarize, our results show that $>70\%$ of the neutrons observed in these shots originate in a plasmoid with n in the range of $3\text{-}4 \times 10^{19}$ cm^{-3}, with radii of about $500\,\mu m$ and lengths of about 1.5 mm, confined ion average E_i up to 160 keV and lifetimes of 30–60 ns.

IV. DISCUSSION

It is useful to compare the thermal with the magnetic energy density in these plasmoids. In the case that electron energy is equal to ion energy, thermal energy density is $\sim 2 \times 10^{13}$ erg/cm^3. If we take the plasmoid magnetic field to be generated by a solenoid with ~ 10 turns and length 1.5 mm, as indicated in Fig. 6, for the peak current of 1 MA, B is ~ 80 MG and magnetic energy density is 3×10^{14} erg/cm^3 or about 15 times thermal energy density, so is sufficient to confine this hot plasma. In actuality, the average field in the plasmoid as a whole is necessarily less. A minimum estimate can be derived from the energy measured in the ion beams, which must derive their energy from the magnetic field energy stored in the plasmoid. Since the ion beam total energy is ~ 1 kJ for the largest shots, total electron plus ion beam energy must be ~ 2 kJ. For the volume of the plasmoids observed, this gives a minimum magnetic energy density of 1.7×10^{13} erg/cm^3, comparable to thermal energy density. Actual magnetic energy must be more than this, assuming less than 100% efficiency in beam generation.

The results reported here are broadly consistent with earlier reports by Nardi, Bostick, Brzosko *et al.*[6,7] of plasmoids with radii on the order of $100\,\mu m$, n $> 10^{21}$ cm^{-3} and highly energetic confined ions, as well as in the results reported by one of us (Lerner[23]) of plasmoids with n $> 10^{21}$ cm^{-3} and E_i > 100 keV. However, our present results go beyond this earlier work in that we have for the first time obtained high-resolution images of the plasmoid simultaneous with time-of-flight and anisotropy data showing the confinement of ~ 160 keV ions. In addition, we extend the results obtained earlier with total neutron yields of up to 2×10^9 in the case of Bostick, Nardi, Brzosko *et al.*[6,7] and 3×10^{10} neutrons for Lerner to the higher range of $>10^{11}$ neutrons/shot. We have also demonstrated the very clear and significant correlation of E_i with P. However, in these results, we have not yet duplicated the n $> 10^{21}$ cm^{-3} densities of the earlier work.

Our results contrast in some ways with those obtained by Kubes[8] with the PF-1000 machine, where that group observed much larger plasmoids with radii of 6-7 mm compared with our $500\,\mu m$, and lengths of 3–5 cm compared with our 1.5 mm. They also observed multiple neutron pulses with high anisotropy, and the majority of the neutrons being produced by unconfined beam-target interactions. We do not believe this to be a contradiction, as both our results and the earlier ones at Texas A&M were obtained on DPFs with small cathode radii of 5–8 cm. In contrast, the PF-1000 has a cathode radius of 20 cm and anode radius of 10 cm.

There are theoretical reasons[4] to believe that plasmoid radii increase with increased electrode radii, and therefore the use of smaller electrodes for the same peak current (higher initial magnetic field) increases both the density of the plasmoids and the total fusion yield for the same input current.

The conditions obtained in these experiments with deuterium are of interest for aneutronic fusion, such as pB11. At 150 keV, for example, the reaction cross section of the reaction p+B$_{11}\rightarrow$3 He$_4$ is almost triple that of DD, such that similar conditions would yield $\sim 4 \times 10^{11}$ pB11 reactions in the best shots.

Previous theoretical work has shown that there are effects at high magnetic fields that can reduce x-ray Bremsstrahlung with pB11 plasma.[26] Simulation[31] has also indicated promise that fusion power may at times exceed x-ray emission. We intend to test this soon.

[1]F. Castillo Mejla, M. Milanese, R. Moroso, and J. Pouzo, J. Phys. D: Appl. Phys. **30**, 1499 (1997).

[2]V. Nardi, W. H. Bostick, J. Feugeas, and W. Prior, Phys. Rev. A **22**, 2211 (1980).

[3]K. N. Koshelev, V. I. Krauz, N. G. Reshetniak, R. G. Salukvadze, Yu. V. Sidelnikov, and E. Yu Khautiev, J. Phys. D: Appl. Phys. **21**, 1827 (1988).

[4]W. H. Bostick, V. Nardi, and W. Pryor, J. Plasma Phys. **8**, 7 (1973).

[5]M. Sadowski, H. Herold, H. Schmidt, and M. Shakhatre, Phys. Lett. A **105**, 117 (1984).

[6]W. H. Bostick, V. Nardi, and W. Prior, Ann. N.Y. Acad. Sci. **251**, 2 (1975).

[7]J. S. Brzosko and V. Nardi, Phys. Lett. A, **155**, 162 (1991).

[8]P. Kubes, J. Kravarik, D. Klir, K. Rezac, M. Scholz, M. Paduch, I. Ivanova-Stanik, L. Karpinski, K. Tomaszewski, and J. M. Sadowski, IEEE Trans. Plasma Sci. **39**, 562 (2011).

[9]C. R. Haas, G. Herziger, R. Lebert, and R. Noll, in *Proceedings of 3rd International Workshop on Plasma Focus* (Institut für Plasmaforschung - Universität Stuttgart, Stuttgart, Germany, 1983), p. 87.

[10]G. Herziger, R. Noll, K. Ruehl, K. Schmitt, L. Michel, and H. Krompholz, in *Proceedings of International Conference on Plasma Physics*, 2–3 July 1984 (Ecole polytechnique federal de Lausanne, Lausanne, 1984), p. 31.

[11]H. Schmidt, in *Proceedings of 3rd International Workshop on Plasma Focus* (Institut für Plasmaforschung - Universität Stuttgart, Stuttgart, Germany, 1983), pp. 63–66.

[12]K. N. Koshelev, G. Salukvadze, Yu V. Sidelnikov, and E. Yu Khautiev, J. Phys. D **21**, 1827 (1988).

[13]L. Bertalot, R. Deutsch, H. Herold, U. Jager, H. J. Kaeppeler, A. Mozer, T. Oppenlander, R. Ruckle, M. Sadowski, P. Schilling, and H. Schmidt, "Experiments on plasma focus dynamics, neutron production and ion emission," in *IAEA Plasma Physics and Controlled Nuclear Fusion, International Conference*, Brussels, 1–10 July 1980 (IAEA, Vienna, 1980), p. 177.

[14]J. S. Brzosko, V. Nardi, J. R. Brzosko, and D. Goldstein, Phys. Lett. A **192**, 250 (1994).

[15]J. S. Brzosko, J. R. Brzosko, B. V. Robouch, and Luigi Ingrosso, Phys. Plasmas **2**, 1259 (1995).

[16]G. R. Neil and R. S. Post, Plasma Phys. **14**, 425 (1988).

[17]I. V. Volobuev, V. A. Gribkov, D. Denus, N. V. Kalachev, T. A. Kolzlova, O. N. Krokhin, S. Sledziński, S. A. Startsev, and S. Czekaj, Sov. J. Plasma Phys. **14**, 401 (1988).

[18]K. Hirano, K. Shimoda, T. Yamamoto, M. Sato, K. Kobayashi, and H. Misaizu, in *Proceedings of 11th Europe Conference Controlled Fusion and Plasma Physics*, Aachen, 5–9 September 1983 (European Physics Society, Geneva, 1983), Vol. 1, p. 551.

[19]L. Jakubowski, M. Sadowski, and J. Zebrowksi, Nucl. Fusion **41**, 755 (2001).

[20]L. Bertalot, H. Herold, U. Jäger, A. Mozer, T. Oppenländer, M. Sadowski, and H. Schmidt, Phys. Lett A **79**, 389 (1980).

[21]E. J. Lerner, Laser Part. Beams **4**(2), 193 (1986).

[22]E. J. Lerner and A. L. Peratt, Final Report, Jet Propulsion Laboratory contract No. 959962, 1995.

[23]E. J. Lerner, in *Current Trends in International Fusion Research—Proceedings of the Fifth Symposium*, edited by E. Panarella, NRC (Research Press, National Research Council of Canada, Ottawa, ON K1A 0R6 Canada, 2007).

[24]Method and apparatus for producing x-rays, ion beams and nuclear fusion energy, U.S. patent 7,482,607 (2009).

[25]E. J. Lerner and R. E. Terry, Current Trends in International Fusion Research—Proceedings of the Sixth Symposium, (National Research Council of Canada, 2009), p. 11.

[26]E. J. Lerner, S. K. Murali, and A. Haboub, J. Fusion Energy **30**, 367 (2011).

[27]F. J. Goldin, B. T. Meehan, E. C. Hagen, and P. R. Wilkins, Rev. Sci. Instrum. **81**, 10E531 (2010).

[28]S. P. Bogdanov and V. I. Volosov, "Recent advances in plasma diagnostics," in *Corpuscular, Correlation, Bolometric, and Other Techniques*, edited by V. T. Tolok (Consultants Bureau, New York, 1971), Vol. 3, p. 1.

[29]M. M. Milanese and J. O. Pouzo, Nucl. Fusion **18**, 533 (1978).

[30]E. J. Lerner, S. Krupakar Murali, A. Blake, D. Shannon, and F. Van Roessel, "Fusion reaction scaling in a mega-amp dense plasma focus," Nucleonika (submitted).

[31]H. R. Yousefi, T. Haruki, J. I. Sakai, A. Lumanta, and K. Masugata, Phys. Lett. A **373**, 2360 (2009).